Ionospheric Climatology Over a Complete Solar Cycle Observed Using Amateur Radio Contact Data

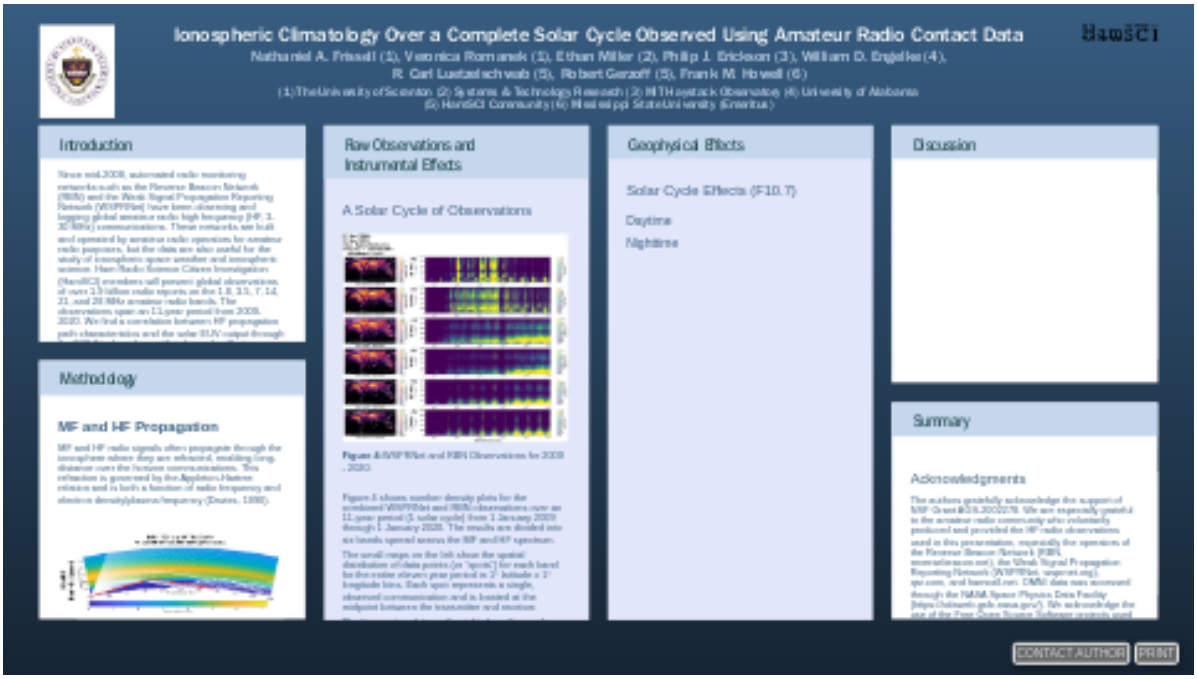

Nathaniel A. Frissell (1), Veronica Romanek (1), Ethan Miller (2), Philip J. Erickson (3), William D. Engelke (4),
R. Carl Luetzelschwab (5), Robert Gerzoff (5), Frank M. Howell (6)

(1) The University of Scranton (2) Systems & Technology Research (3) MIT Haystack Observatory (4) University of Alabama
(5) HamSCI Community (6) Mississippi State University (Emeritus)

PRESENTED AT:

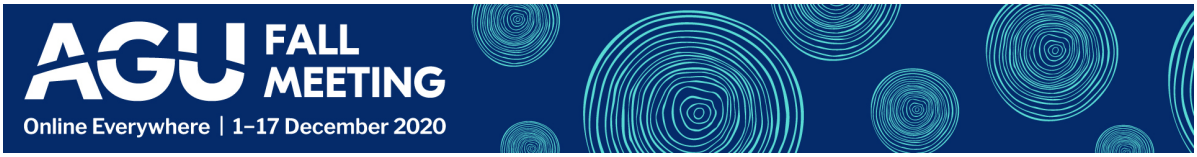

INTRODUCTION

Since mid-2008, automated radio monitoring networks such as the Reverse Beacon Network (RBN) and the Weak Signal Propagation Reporting Network (WSPRNet) have been observing and logging global amateur radio high frequency (HF, 3-30 MHz) communications. These networks are built and operated by amateur radio operators for amateur radio purposes, but the data are also useful for the study of ionospheric space weather and ionospheric science. Ham Radio Science Citizen Investigation (HamSCI) members will present global observations of over 1.9 billion radio reports on the 1.8, 3.5, 7, 14, 21, and 28 MHz amateur radio bands. The observations span an 11-year period from 2009-2020. We find a correlation between HF propagation path characteristics and the solar EUV output through the F10.7 index, along with solar cycle effects, seasonal effects, and sporadic E signatures. We will also discuss impacts of operator behavior and sampling effects caused by the distribution of amateur radio transmitting and receiving stations.

METHODOLOGY

MF and HF Propagation

MF and HF radio signals often propagate through the ionosphere where they are refracted, enabling long-distance over the horizon communications. This refraction is governed by the Appleton-Hartree relation and is both a function of radio frequency and electron density/plasma frequency (Davies, 1990).

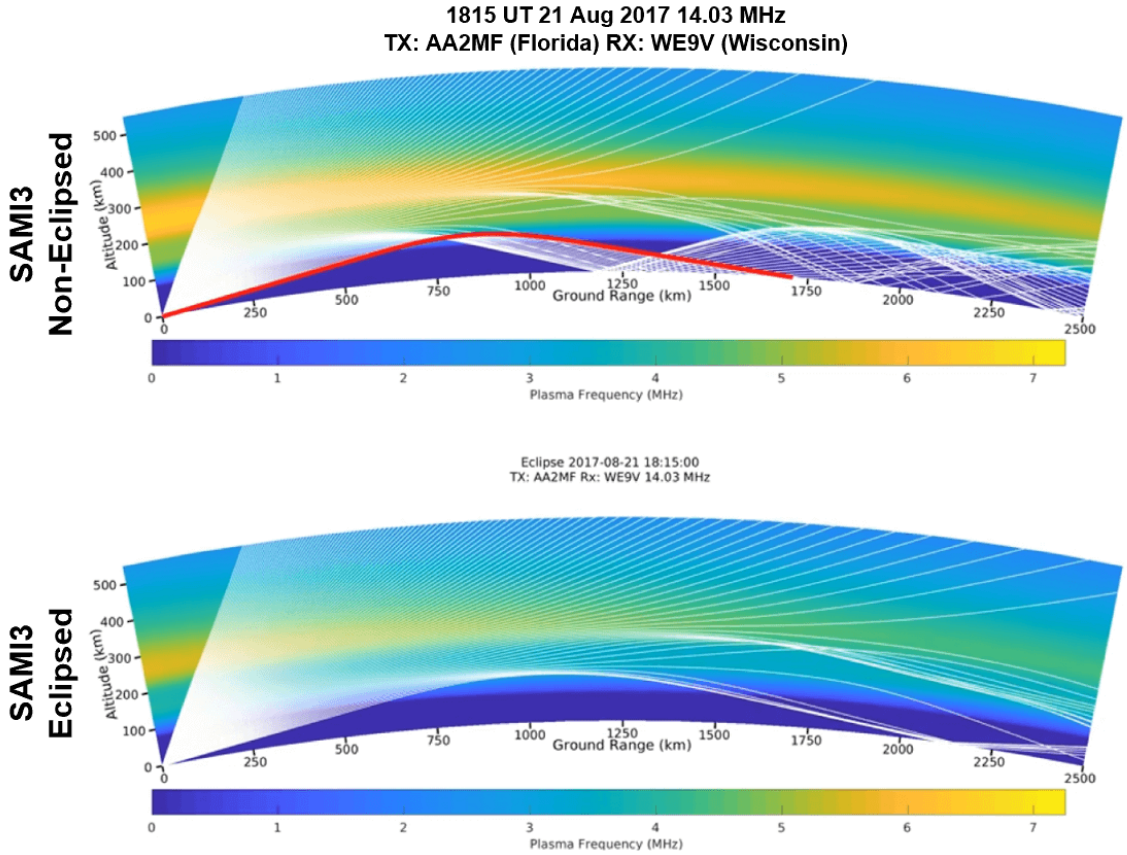

Figure 1: An example of HF propagation where the radio frequency is held constant, but the electron density (plasma frequency) varies. Both panels show a raytrace of a 14.03 MHz radio signal from a transmitter in Florida towards a receiver in Wisconsin made with the PHaRLAP raytracing toolkit (Cervera & Harris, 2014) on 21 August 2017 at 1815 UT. The electron densities in the top panel come from a standard run of the SAMI3 model ionosphere. The red line indicates a predicted radio path from the transmitter to receiver. The electron densities in the bottom panel are from a run of SAMI3 that includes the Solar Eclipse occurring on that day (Frissell et al., 2018; Huba & Drob, 2017), and therefore reduced compared to the top panel. The 14.03 MHz signal undergoes less refraction in this case, and therefore skips over the receiver in Wisconsin.

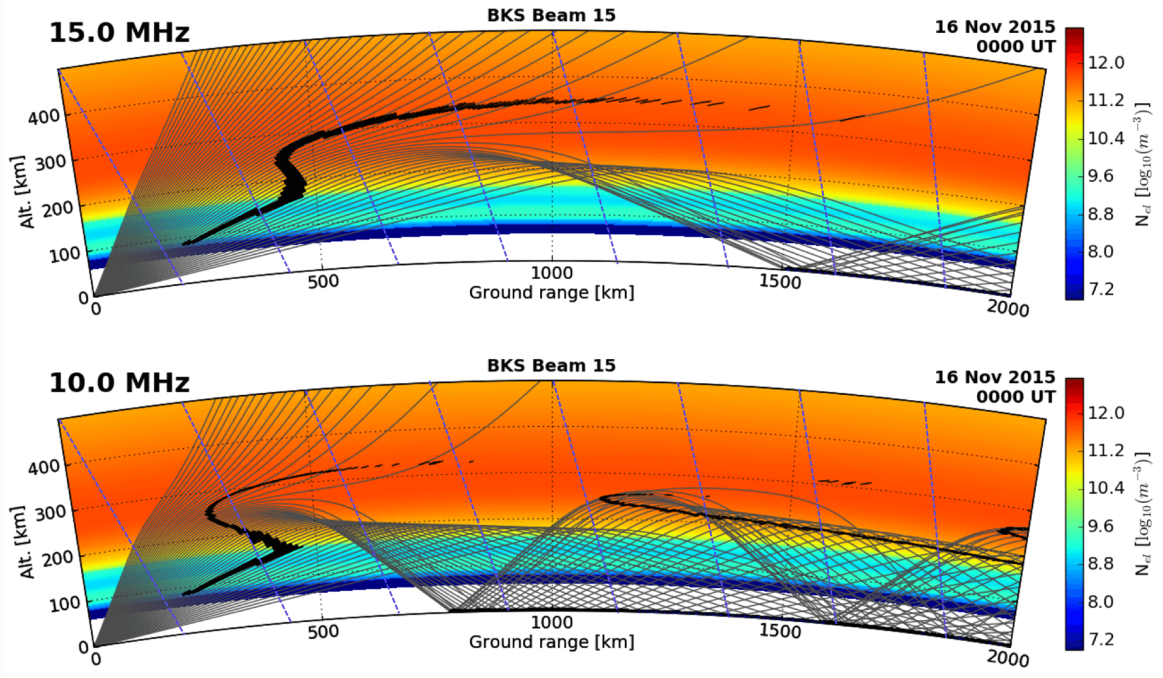

Figure 2: An example of HF propagation where the ionospheric electron densities are held constant, but the transmitter frequency varies. Both figures show a raytrace of transmissions from the Blackstone, Virginia SuperDARN radar along a northeast heading. Background densities are from the International Reference Ionosphere (IRI) (Bilitza et al., 2011). The top panel uses a transmit frequency of 15 MHz and shows significantly more refraction than the bottom panel, which uses a transmit frequency of 10 MHz. Figure from Frissell, 2016.

Frequencies Utilized

In this study, we use observations of radio communications on selected medium frequency (MF, 0.3 – 3 MHz) and high frequency (HF, 3 – 30 MHz) amateur radio bands. The six bands selected are shown in the table below.

Table 1: Selected MF and HF amateur radio bands used in this study.

	Band Name (Approx. Wavelength)	US Amateur Radio Frequency Limits
MF Medium Frequency	160 m	1.8 – 2.0 MHz
HF High Frequency	80 m	3.5 – 4.0 MHz
	40 m	7.0 – 7.3 MHz
	20 m	14.0 – 14.35 MHz
	15 m	21.0 – 21.45 MHz
	10 m	29.0 – 29.7 MHz

Amateur Radio Observation Networks

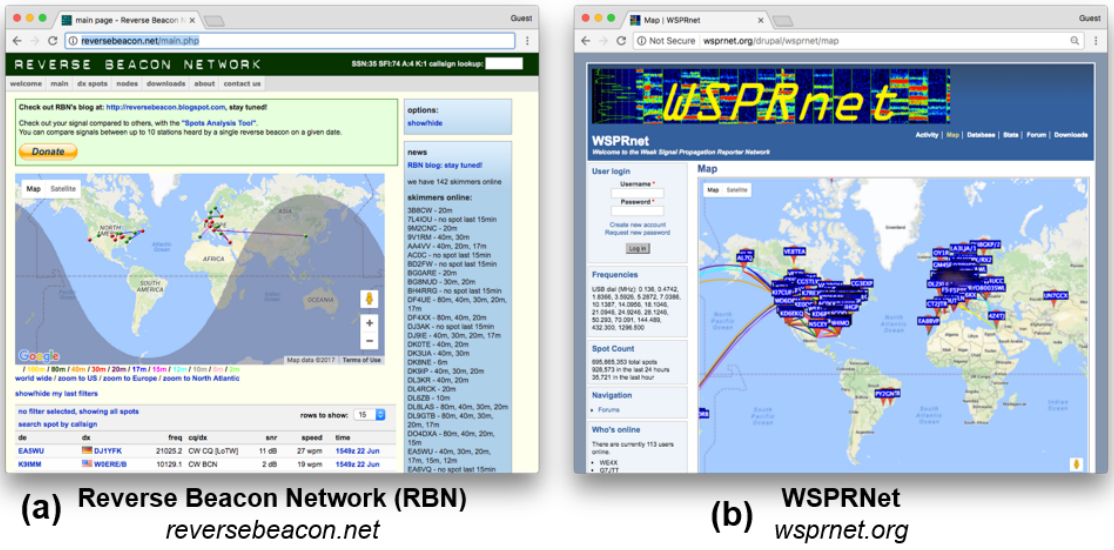

Figure 3: Amateur radio observation networks used in this study.

Two sources of amateur radio observation data were used in this study: The Reverse Beacon Network (RBN, reversebeacon.net) (http://www.reversebeacon.net/main.php) and the Weak Signal Propagation Reporter Network (WSPRNet, wsprnet.org) (http://wsprnet.org/).

The RBN in a global network of HF software defined radio (SDR) receivers capable of automatically decoding amateur Morse Code (a.k.a. Continuous Wave CW) and radio teletype (RTTY) transmissions. The RBN relies on volunteer, continuously operating receivers located at fixed locations (Frissell et al., 2014). Station location data for RBN observations is obtained by looking up station call signs in the http://qrz.com (https://www.qrz.com/) and http://hamcall.net (https://hamcall.net/) amateur radio databases.

Weak Signal Propagation Reporter (WSPR) is an amateur radio digital mode designed by Joe Taylor for the purpose of testing low-power propagation paths on the MF and HF bands (Taylor & Walker, 2010). WSPRNet.org is the website that aggregates all of the observations from this network.

RAW OBSERVATIONS AND INSTRUMENTAL EFFECTS

A Solar Cycle of Observations

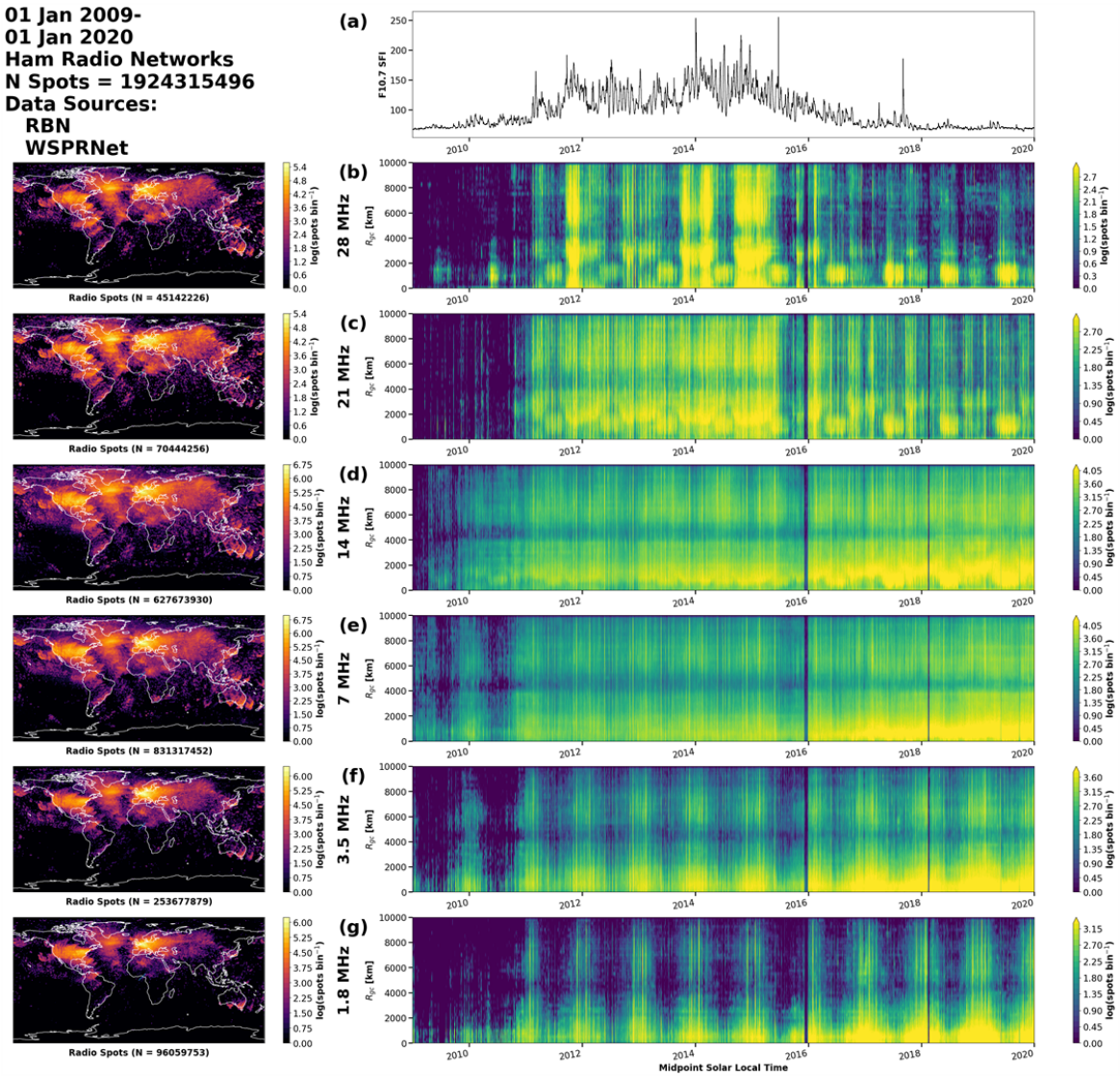

Figure 4: WSPRNet and RBN Observations for 2009 – 2020 with F10.7 Solar Flux Index on top.

Figure 4 shows number density plots for the combined WSPRNet and RBN observations over an 11-year period (1 solar cycle) from 1 January 2009 through 1 January 2020. The results are divided into six bands spread across the MF and HF spectrum.

The small maps on the left show the spatial distribution of data points (or “spots”) for each band for the entire eleven year period in 1° latitude x 1° longitude bins. Each spot represents a single, observed communication and is located at the midpoint between the transmitter and receiver.

The time series plots on the right show the number density of spots as function of time. The y-axis gives the great circle ground range between the transmitter and receiver. Data have been binned into 250 km x 3 hr bins and plotted using the local time (UT + 15°/longitude) of the spot.

The structures observed in Figure 4 are the result of multiple factors, including solar cycle and geophysical influences, the geographic distribution of the transmitters and receivers, and the variation of the number of participating stations with time.

Geographic Distribution of Transmitters and Receivers

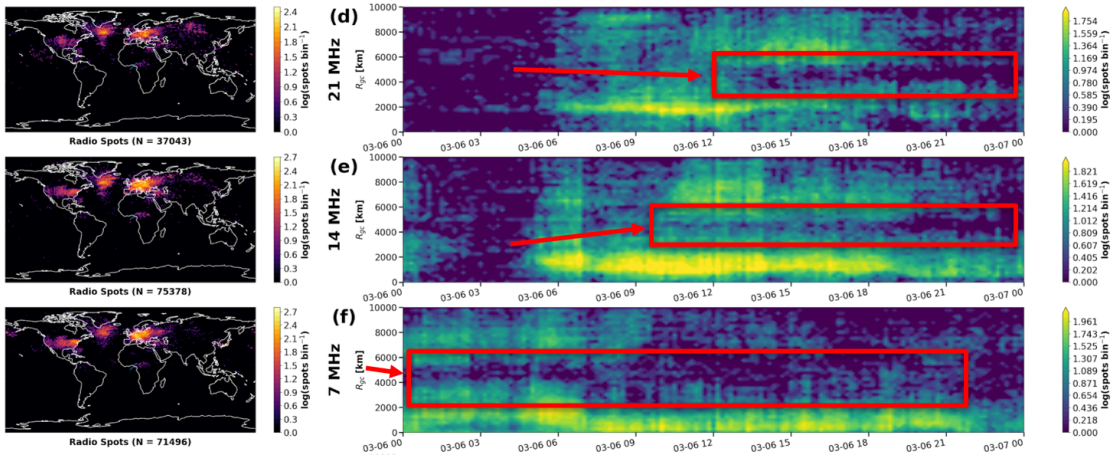

Figure 5: RBN and WSPR observations for 6 March 2016. The red boxes highlight a data gap between about 4000 to 6000 km ground range commonly observed on all bands in the data. This gap is also apparent in Figure 4 for all 11 years.

A gap in the ground range distribution of the RBN and WSPRNet data from approximately 4000 to 6000 km appears in all bands in Figure 4 and Figure 5. It is likely this gap is due to one of two causes: (1) Geographic distribution of the transmitters and receivers, or (2) a skip zone due to ionospheric propagation.

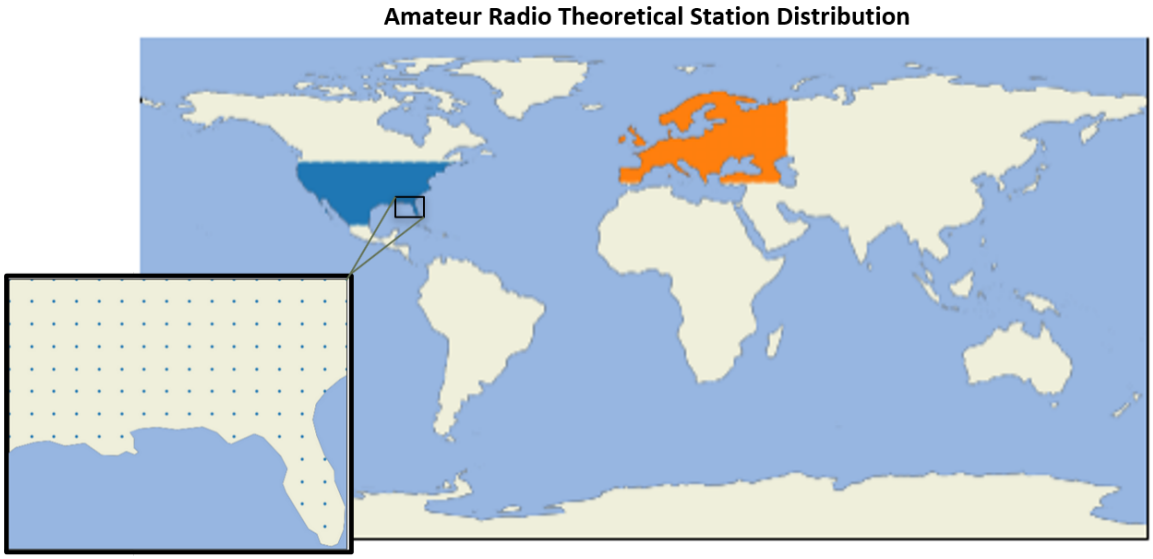

Figure 6: Grid of theoretical station locations used in computing the probability of observing a particular ground range Rgc. Individual stations are arranged in a 10° lat x 10° lon grid.

We test hypothesis (1) by calculating the probability of observing a particular ground range. This was calculated by computing every combination of ground ranges among a theoretical grid of stations. We set the following assumptions and conditions in our simulation, which are illustrated in Figure 6:

- The majority of active stations are in the continental US or Europe.
- Stations are equally spaced in a grid with 10° lat x 10° lon spacing

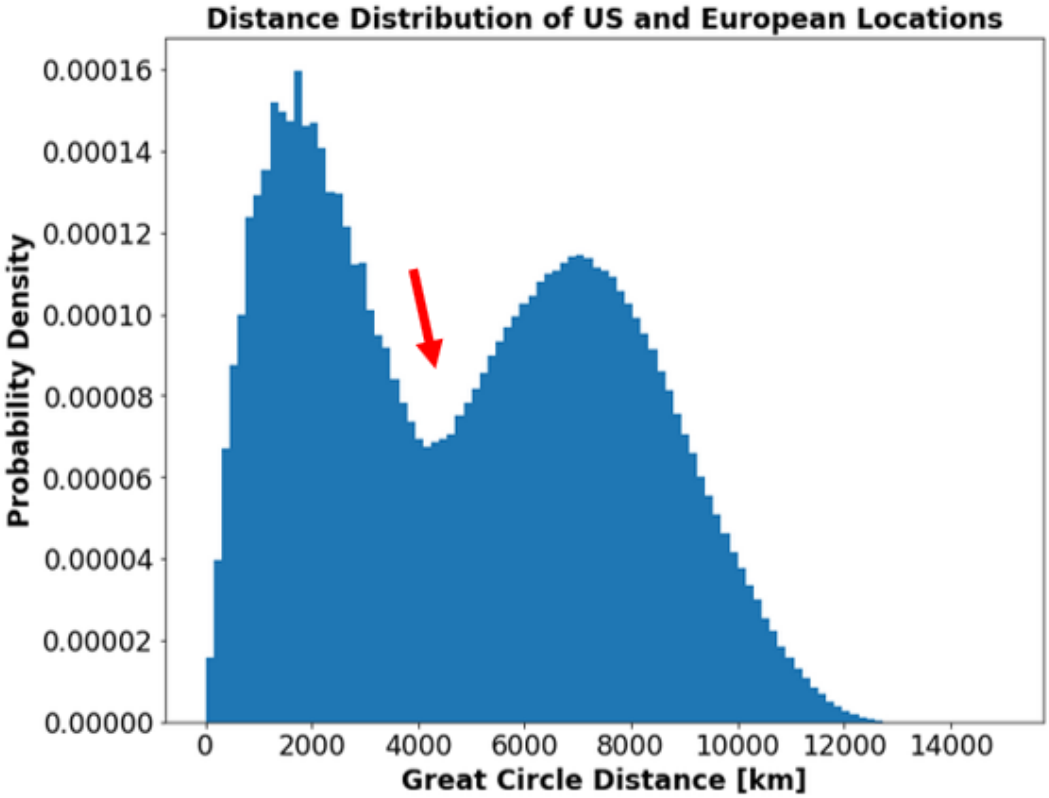

Figure 7: Computed probability distribution function of observing a particular great circle distance Rgc with the RBN/WSPRNet.

Figure 7 shows the result of the simulation, the probability distribution function of observing a particular great circle distance Rgc with the RBN/WSPRNet assuming an equally-spaced grid of stations in the continental US and Europe. The result is a bi-modal distribution that shows approximately a 25% to 50% decrease in probability of observing communications distances between 4000 to 6000 km as compared to peaks at 2000 and 8000 km. This suggests that geographic distribution of stations (largely due to the Atlantic Ocean) is a significant cause of the gaps between 4000 to 6000 km seen in Figure 4 and Figure 5.

GEOPHYSICAL EFFECTS

Solar Cycle Effects (F10.7)

Daytime

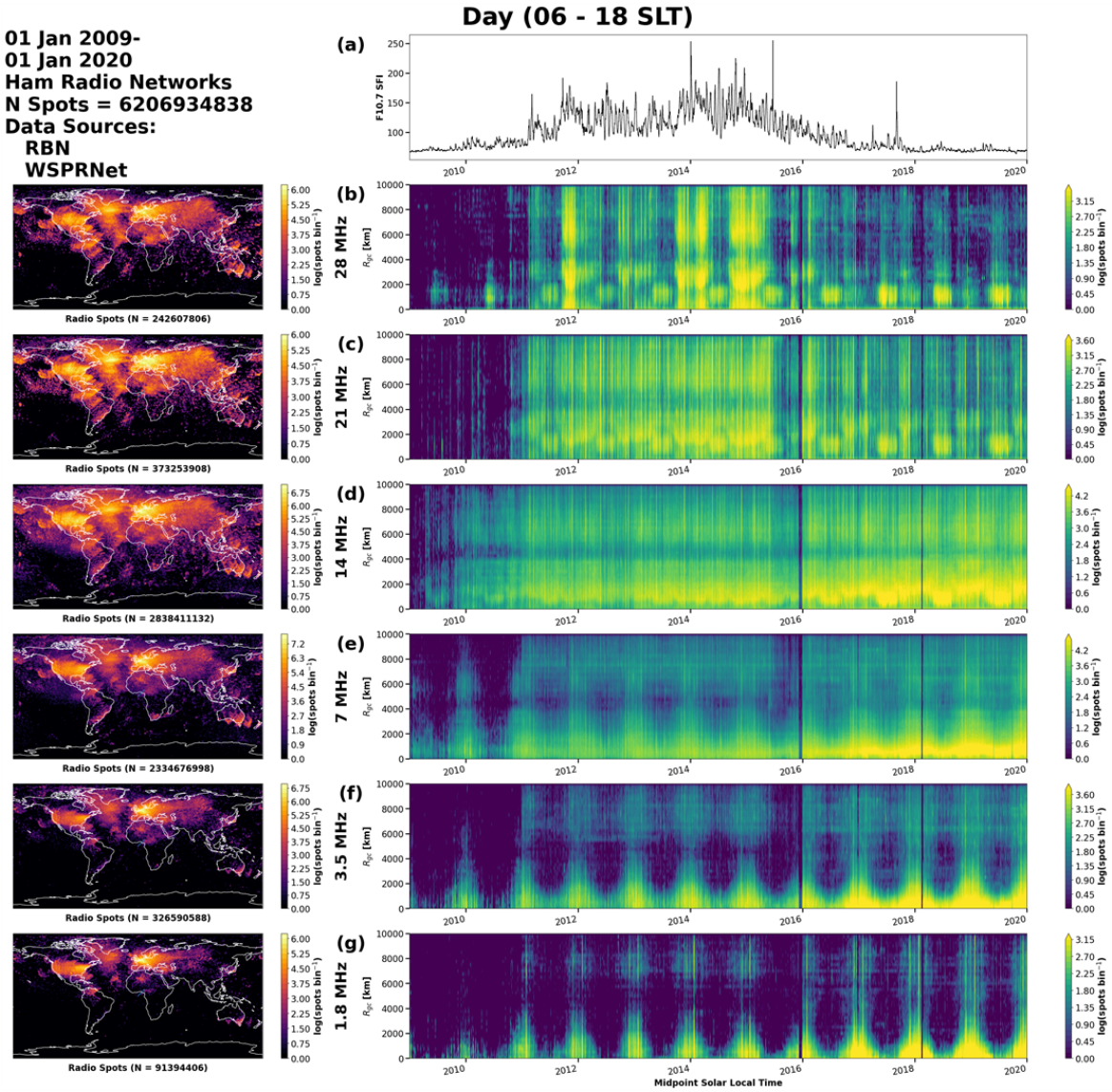

Figure 8: Daytime propagation for WSPRNet and RBN Observations for 2009 – 2020. The F10.7 Solar Flux Index is shown in panel (a). In this figure, only spots where the midpoint between the transmitter and receiver has a solar local time between 06 to 18 is shown.

Nighttime

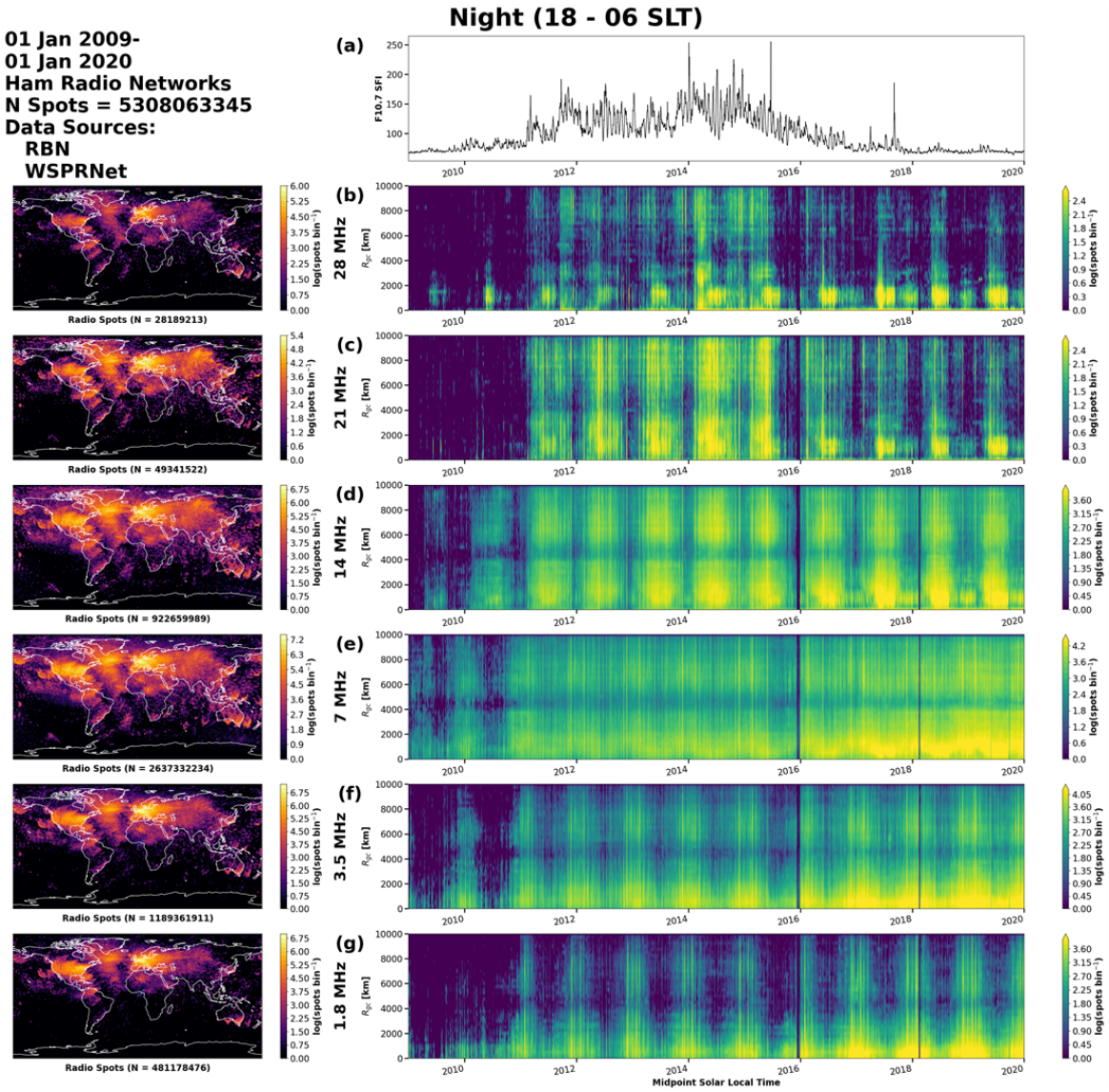

Figure 9: Nighttime propagation for WSPRNet and RBN Observations for 2009 – 2020. The F10.7 Solar Flux Index is shown in panel (a). In this figure, only spots where the midpoint between the transmitter and receiver has a solar local time between 18 to 06 is shown.

DISCUSSION

Solar Cycle Effects

Figure 4 shows a strong correlation between the F10.7 index and amateur radio activity, particularly on the 21 and 28 MHz bands. This is most prevalent when F10.7 is greater than 100, between the years 2011 and 2016. During this time, long-distance propagation > 4000 km is a common occurrence on 21 and 28 MHz. This > 4000 km propagation is much less prevalent prior to 2011 and after 2016, when F10.7 is typically < 100. Figure 4 also shows that during the peak of the solar cycle, shorter duration enhancements in F10.7 can also lead to strong enhancements on 28 MHz. This is observed most clearly towards the end of 2011, the end of 2013, the beginning of 204, and throughout most of 2015. These observations are consistent with an increase in ionospheric densities, and hence the maximum usable frequency, associated with enhanced solar activity.

Diurnal Variations

Figures 8 and 9 compare day versus night propagation from 2011 through 2020. The most significant difference between the two is that higher frequencies (14, 21, and 28 MHz) show more activity, while lower frequencies (1.8, 3.5, and 7 MHz) show more activity at night. The lower frequencies also show longer distance propagation at night. This is consistent with enhanced photoionization during the daylight hours followed by recombination during darkness.

Seasonal Variations

Seasonal effects are also observed in the data. The maps show that the spatial distribution of spots is weighted to the Northern hemisphere, and therefore Northern hemisphere seasonal trends appear in the data. In Figures 4, 8, and 9, 1.8 and 3 MHz show most activity in the winter, as the majority of the spots are centered around the yearly tick marks, which fall on January 1 of each year. Conversely, summer effects are seen most strongly on 14, 21, and 28 MHz at night in Figure 9. These bands show a clear decrease in spot density on January 1 of each year. The 14, 21, and 28 MHz bands do not show a clear seasonal effect during the day in Figure 8, as ionospheric densities are more likely to remain high enough to support propagation on these bands during the day throughout the year.

Instrumental Effects

Every frequency band shown in Figures 4, 8, and 9 show a gap in observed communications between ranges of about 4000 to 6000 km. Using a simulated set of transmitters and receivers distributed evenly throughout the continental United States and Europe, we have shown that this is gap is likely due to the geographic distribution of stations.

Additionally, Figures 4, 8, and 9 show a general increase in the number of spots observed from 2011 through 2020. This is likely due to the increase in the number of amateurs participating in both RBN and WSPRNet. To help mitigate the effect of this trend on our conclusions, we have presented Figures 4, 8, and 9 using a logarithmic colormap to increase the dynamic range of the visualization. We have also not made any conclusions regarding the increase in spots on the low bands (1.8, 3.5, and 7 MHz) at the end of the solar cycle from 2016 – 2020. In the future, we intend to develop a systematic method of normalizing for the number of contributing stations.

Finally, there are some data gaps in the presented figures that can be attributed to missing data due to challenges in data aggregation and processing. These will be addressed in future work.

SUMMARY

Summary and Future Work

In this poster, we have presented data from the Reverse Beacon Network (RBN) and the Weak Signal Propagation Reporting Network (WSPRNet) automated amateur radio high frequency (HF) communications observing networks from 2009 - 2020. We have found that amateur radio activity is strongly correlated with F10.7 solar flux on the 21 and 28 MHz bands. A strong diurnal variation is observed, the higher bands (14, 21, and 28 MHz) more active during the day, and the lower bands (1.8, 3.5, and 7 MHz) are more active at night. Seasonal variations are also observed, with the lower bands more active during Northern Hemisphere Winter and high bands more active during the Northern Hemisphere Summer.

Instrumental effects were also observed, particularly a gap in observations at ranges between about 4000 to 6000 km on all bands that can be attributed primarily to the geographic distribution of participating stations. A general trend of increasing number of spots with time is likely attributable to an increase in the number of participating stations. Future work will be to develop a method of systematically normalizing for the number of participating station, as well as address data gaps due to challenges in data aggregation and processing.

Acknowledgments

The authors gratefully acknowledge the support of NSF Grant AGS-2002278. We are especially grateful to the amateur radio community who voluntarily produced and provided the HF radio observations used in this presentation, especially the operators of the Reverse Beacon Network (RBN, reversebeacon.net), the Weak Signal Propagation Reporting Network (WSPRNet, wsprnet.org), qrz.com, and hamcall.net. OMNI data was accessed through the NASA Space Physics Data Facility (https://omniweb.gsfc.nasa.gov/). We acknowledge the use of the Free Open Source Software projects used in this analysis: Ubuntu Linux, python, matplotlib, NumPy, SciPy, pandas, xarray, iPython, and others.

REFERENCES

American Radio Relay League. (2015). US Amateur Radio Numbers Reach an All-Time High. http://www.arrl.org/news/us-amateur-radio-numbers-reach-an-all-time-high

Bilitza, D., McKinnell, L.-A., Reinisch, B., & Fuller-Rowell, T. (2011). The international reference ionosphere today and in the future. Journal of Geodesy, 85(12), 909–920. https://doi.org/10.1007/s00190-010-0427-x (http://dx.doi.org/10.1007/s00190-010-0427-x)

Cervera, M. A., & Harris, T. J. (2014). Modeling ionospheric disturbance features in quasi-vertically incident ionograms using 3-D magnetoionic ray tracing and atmospheric gravity waves. Journal of Geophysical Research: Space Physics, 119(1), 431–440. https://doi.org/10.1002/2013JA019247 (http://dx.doi.org/10.1002/2013JA019247)

Davies, K. (1990). Ionospheric Radio. Peter Peregrinus Ltd.

Frissell, N. A. (2016). Ionospheric Disturbances: Midlatitude Pi2 Magnetospheric ULF Pulsations and Medium Scale Traveling Ionospheric Disturbances [Virginia Tech]. http://hdl.handle.net/10919/74976

Frissell, N. A., Katz, J. D., Gunning, S. W., Vega, J. S., Gerrard, A. J., Earle, G. D., Moses, M. L., West, M. L., Huba, J. D., Erickson, P. J., Miller, E. S., Gerzoff, R. B., Liles, W., & Silver, H. W. (2018). Modeling Amateur Radio Soundings of the Ionospheric Response to the 2017 Great American Eclipse. Geophysical Research Letters, 45(10), 4665–4674. https://doi.org/10.1029/2018GL077324 (http://dx.doi.org/10.1029/2018GL077324)

Frissell, N. A., Miller, E. S., Kaeppler, S. R., Ceglia, F., Pascoe, D., Sinanis, N., Smith, P., Williams, R., & Shovkoplyas, A. (2014). Ionospheric Sounding Using Real-Time Amateur Radio Reporting Networks. Space Weather, 12(12). https://doi.org/http://dx.doi.org/10.1002/2014SW001132 (http://dx.doi.org/10.1002/2014SW001132)

Frissell, N. A., Vega, J. S., Markowitz, E., Gerrard, A. J., Engelke, W. D., Erickson, P. J., Miller, E. S., Luetzelschwab, R. C., & Bortnik, J. (2019). High-Frequency Communications Response to Solar Activity in September 2017 as Observed by Amateur Radio Networks. Space Weather, 17(1), 118–132. https://doi.org/10.1029/2018SW002008 (http://dx.doi.org/10.1029/2018SW002008)

Huba, J. D., & Drob, D. (2017). SAMI3 prediction of the impact of the 21 August 2017 total solar eclipse on the ionosphere/plasmasphere system. Geophysical Research Letters, 44(12), 5928–5935. https://doi.org/10.1002/2017GL073549 (http://dx.doi.org/10.1002/2017GL073549)

Taylor, J., & Walker, B. (2010). WSPRing Around the World. QST, 94(11), 30–32.